Exploration of Carbon Nanotube Forest Synthesis-Structure Relationships Using Physics-Based Simulation and Machine Learning

Taher Hajilounezhad†, Zakariya A. Oraibi‡, Ramakrishna Surya⋆,
Filiz Bunyak‡, Matthew R. Maschmann†, Prasad Calyam‡, Kannappan Palaniappan‡
†Mechanical & Aerospace Engineering, University of Missouri, Columbia, MO 65211 USA
‡Electrical Engineering and Computer Science, University of Missouri, Columbia, MO 65211 USA
⋆Material Science and Engineering, University of Cincinnati, Cincinnati, OH 45221 USA

***Abstract*—The parameter space of CNT forest synthesis is vast and multidimensional, making experimental and/or numerical exploration of the synthesis prohibitive. We propose a more practical approach to explore the synthesis-process relationships of CNT forests using machine learning (ML) algorithms to infer the underlying complex physical processes. Currently, no such ML model linking CNT forest morphology to synthesis parameters has been demonstrated. In the current work, we use a physics-based numerical model to generate CNT forest morphology images with known synthesis parameters to train such a ML algorithm. The CNT forest synthesis variables of CNT diameter and CNT number densities are varied to generate a total of 12 distinct CNT forest classes. Images of the resultant CNT forests at different time steps during the growth and self-assembly process are then used as the training dataset. Based on the CNT forest structural morphology, multiple single and combined histogram-based texture descriptors are used as features to build a random forest (RF) classifier to predict class labels based on correlation of CNT forest physical attributes with the growth parameters. The machine learning model achieved an accuracy of up to 83.5% on predicting the synthesis conditions of CNT number density and diameter. These results are the first step towards rapidly characterizing CNT forest attributes using machine learning. Identifying the relevant process-structure interactions for the CNT forests using physics-based simulations and machine learning could rapidly advance the design, development, and adoption of CNT forest applications with varied morphologies and properties.**

Keywords: Finite Element, Simulation, Carbon Nanotubes, Local Feature Extraction, Random Forests, Classification.

I. Introduction

Carbon nanotubes (CNTs) are widely studied for their promising mechanical, electrical, and thermal properties [1] that make them suitable for diverse applications including photodetectors [2], thin-film flexible electronics [3] [4], transparent conductive membranes [5], electrocatalysis support [6], bioelectronics [7] and physical sensors [8] [9] [10]. When CNTs are synthesized in dense populations known as CNT forests, however, a significant performance gap between individual CNTs and CNT forests is observed. To date, overcoming the performance gaps has not been achieved due to a lack of understanding about how the processing mechanisms of CNT synthesis control the CNT self-assembly process [9] [11][12][13][14][15][16]. The wavy and entangled morphology of CNT forest caused by the mechanical competition of concurrently growing CNTs during self-assembly process is considered the main source of the performance degradation [17][18][19][20][21][22]. An internal morphology of a relatively straight and a wavy CNT forest is shown in Figure 1.

Achieving a desired property set from CNT forests is currently an unfulfilled challenge. Most CNT synthesis recipes rely on previously successful results rather than a fundamental understanding of CNT forest kinetics and the assembly process. The CNT forest processing parameter space includes numerous variables including catalyst composition, catalyst thickness, synthesis temperature, processing gas composition, synthesis time, operating pressure, among others. An experimental exploration of the full synthesis parameter space is both cost and time prohibitive. Numerical simulation of CNT forests synthesis and self-assembly is an alternative approach that may increase the speed and diversity of synthesis parameters examined. Such simulations can predict both the CNT forest structural morphology and the resulting CNT forest properties. By systematically varying CNT synthesis parameters, one may arrive at a set of conditions that product the desired CNT forest performance metrics such as mechanical stiffness and thermal conductivity.

These desired performance metrics are intricately related to the structural morphology of the CNT forest itself, although the functional relationships between CNT forest structural morphology and CNT forest properties are currently not well understood. For instance, the CNT forest morphology, in terms of CNT length, waviness, and density, may be tuned according to specific applications [23]- thin-film-type transistors require dense and parallel single-walled carbon nanotubes (SWCNTs) to sustain large current [24][25], while their ultralong length enables easy fabrication of numerous devices out of one individual SWCNT and the construction of logic circuits at a single nanotube level [26][27]. Therefore, predicting the combination of processing parameters required to grow

978-1-7281-4732-1/19/$31.00

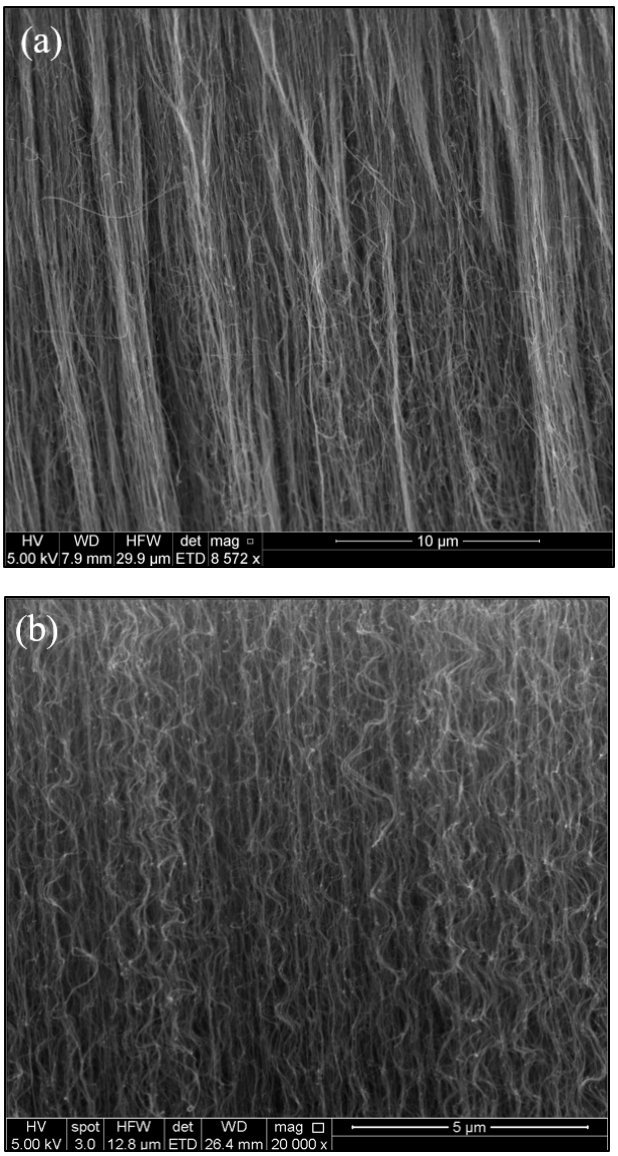

Fig. 1. The internal morphology of a typical (a) relatively straight CNT forest (scale 10 μm) (b) wavy and entangled CNT forest (scale 5 μm).

application-tailored CNT forests would represent a significant advance that could enable new CNT forest-based applications that fully exploit the beneficial properties of individual CNTs. Here we employ a physics-based numerical simulation of CNT forest growth and assembly to generate images of CNT forest morphology using variable synthesis parameters. The simulated imagery is used to train a ML model to predict the growth attributes of a CNT forest.

Machine learning is a powerful technique to identify patterns governing the behavior of nanomaterials synthesis to accelerate the search for optimal materials. Recent developments in the eld of machine learning (ML) combined with the current materials data infrastructure have made the data driven techniques popular and increasingly popular within the materials science community. Machine learning algorithms excel at nding patterns in a dataset and identifying qualitative trends and outliers that would otherwise be extremely difcult to nd. Hence, ML exhibits a great potential in assisting materials design and synthesis in the future with the ambitious goal of accelerated and application-tailored materials design and discovery [28]. Recently, ML is successfully employed to design organic light-emitting diodes [29], metal-organic frameworks [30], drugs [31], classify steel microstructures [32], construction materials [33] and in combination with computational materials to predict graphene bandgap [34]. A paradigm shift in the eld of material science is inevitable in the upcoming years as ML and deep learning (DL) becoming increasingly powerful.

Unfortunately, the amount of available experimental data of CNT forest growth is not sufficient to be used as labeled data for training the machine learning model due to the vast range of CNT forest synthesis conditions, growth recipes and resultant morphologies reported in literature. Experimental results are usually noisy, expensive and time consuming, and the CNT forest attributes (CNT diameter, areal density, growth rate) are poorly characterized and time variant. Therefore, the physics-based simulation of CNT forests may present a reliable and powerful tool for training ML models in the absence of suitable experimental data.

In this study, a time-resolved mechanical simulation model is employed to nucleate and synthesize CNT forests. The finite element model is discussed in detail elsewhere [35][36][37][38]. Here, we have grown CNT forests with different user-defined synthesis inputs, namely CNT number density and CNT outer diameter to evaluate their effect on the forest structure. As there is a vast input parameter space that may result in different morphologies, investigating all process conditions is impractical. In this preliminary study, the resulting forest morphology is used to train a machine learning model to predict synthesis properties. Local feature extractors, individually and in combination, followed by random forest classifier were employed to create the class predictor model. We used four local descriptors that are derived from both Local Binary Pattern (LBP) and Motif Cooccurrence Matrix (MCM) descriptors [39][40][41]. The descriptors are Rotation Invariance Cooccurrence among Local Binary Patterns (RIC-LBP), Joint Adaptive Median Binary Patterns (JAMBP), Joint Motif Labels (JML), and Motif Patterns (MP) encoded with RIC-LBP [40]. The reason behind using multiple local descriptors is to capture more texture features and to ultimately improve the final classification accuracy. This work represents a first step towards an autonomously operating system that can determine the synthesis parameters required to synthesize CNT forests with desired property sets.

II. Methodology

A. CNT Forest Simulation

A time-resolved 2D simulation model is employed to simulate CNT forests. The simulation model is based on the finite-element analysis of concurrently growing CNTs whose mechanical equilibrium is evaluated at discrete time

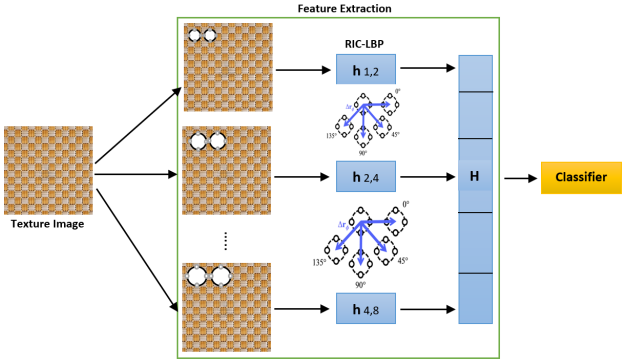

Fig. 2. RIC-LBP Descriptor Computed using Three Different Radius. The Final Histogram is the Concatenation of the Three Radius RIC-LBP Descriptor.

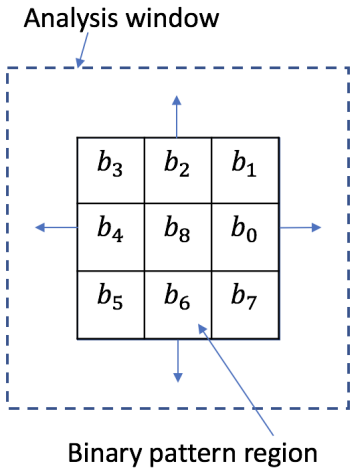

Fig. 3. Illustration of the Adaptive Median Binary Pattern Window.

steps [35][36][37]. Each CNT is modelled as numerous finite frame elements connected end-to-end. The CNT elements are hollow cylinders, each having 6 mechanical degrees of freedom. Three DOF are present at each terminal element node representing axial, transverse, and angular deformation. At each growth step, new elements are added to the bottom of the forest representing a base-growth mechanism. The interactions of neighboring CNTs are approximated by a linearized van der Waals potential when they are in close proximity. The simulation is governed by user-defined inputs such as CNT inner and outer diameter, orientation angle, number density, growth rates, etc. that are assigned at the onset of simulation based on Gaussian distributions.

In this paper, we classify twelve distinct CNT forest classes using different local descriptors to extract the texture features from the CNT forest images. In our proposed framework, the descriptors based on LBP [42] and Motif Peano scan methods [43] are used. The first two descriptors are called RIC-LBP and JAMBP which are a very powerful variation of the original LBP descriptor. The other descriptors are called JML and MP and are a modification of the original MCM descriptor. The reason we choose these set of local features is their ability to capture image texture and the high classification performance generated using challenging databases. In the following, we will explain how each method is used to extract features and the number of features used with respect to each descriptor.

B. LBP-Based Descriptors

1) RIC-LBP: The Rotation Invariant Co-occurrence among LBP (RIC-LBP) proposed by Nosaka et. al [44] was used successfully to classify Human Epithelial type-2 HEp-2 cell images. RIC-LBP makes use of the relationships among the binary patterns by finding the co-occurrence patterns among the histogram features as shown in Figure 2. Moreover, RIC-LBP histogram is represented in the form of many LBP pairs and each pair will be attached with a specific label to account for rotation invariance which makes it very powerful to capture important image texture. As proposed in [44], 408 bins from the three schemes were extracted.

2) JAMBP: The Joint Adaptive Median Binary Patterns (JAMBP) descriptor was introduced in [45] by Hafiane et. al. It builds upon the powerful AMBP [46] descriptor by joining more information extracted from the original image. These information represent the mean of the image and the window size used around each pixel to compute the threshold value. The power of AMBP descriptor is that it uses an adaptive window size around the center pixel as shown in Figure 3. As a result, it has the ability to better capture texture features. Moreover, JAMBP uses multiscale scheme by computing AMBP descriptor using different ranges and sampling points from the center pixel. In our work, we extracted 320 bins from JAMBP and used them in the classification phase.

C. Motif-Based Descriptors

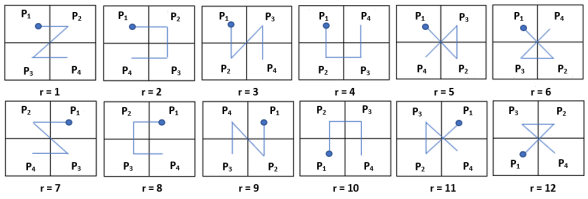

Fig. 4. The Twelve Motif Patterns used in our Approach.

1) JML: The Joint Motif Labels (JML) descriptor was proposed by Oraibi et. al [40]. The descriptor exploits the spatial relationship among intensity pixel in a 2×2 image neighborhood. This is done by finding the Optimum Peano scans among pixels by minimizing the energy of the intensities in a small image region based on the equation below:

$$\delta = |p1 - p2| + |p2 - p3| + |p3 - p4| \quad (1)$$

Figure 4 shows the 12 motif patterns extracted from a

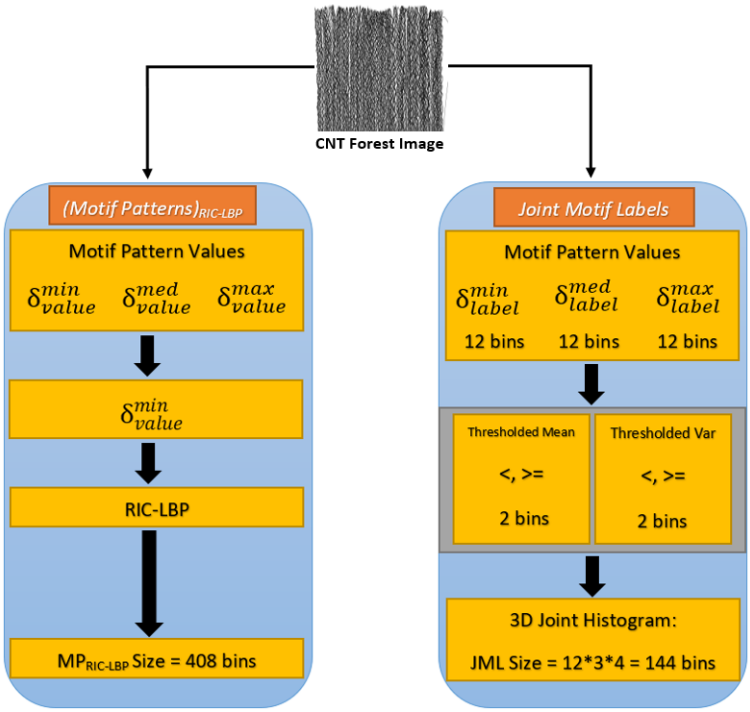

Fig. 5. Feature Vector Calculations of JML and MP Descriptors before Applying the Translational Invariance.

2×2 neighborhood image with the corresponding letters for each pixel that are used in the minimization equation. In order to compute this descriptor, the twelve motif patterns are extracted from the 2×2 neighborhood. Then, these patterns are labeled from 1 - 12. Later, three moments are found: minimum, median, and maximum patterns. Then, the corresponding labels of these patterns are stored in 3 separate matrices. We repeat this process for all image pixels. At the end, we join each matrix with the mean and variance of the image in a 3D joint histogram mechanism. More details can be found in [40]. We also consider the translational invariance property of the descriptor by computing it on four different images: the original one, the original image shifted by one pixel horizontally, vertically, and diagonally by one pixel. As a result, we gain a descriptor that has 576 bins. Figures 5 and 6 illustrate the computation of JML before and after translational invariance.

2) MP: The Motif Patterns (MP) descriptor, which was also proposed by Oraibi et. al [40], works by exploiting the motif patterns extracted during the process of constructing the JML descriptor. These patterns are considered as intensity values since they represent the variation of intensity pixels in a specific neighborhood. As a result, we can exploit these patterns by encoding them using any texture descriptor as shown in Figure 7. We selected the RIC-LBP descriptor to encode the minimum patterns only since it generates powerful features that result in high classification performance. To cope with translational invariance, we applied the same approach as in JML and extracted features from 4 images. The result is a descriptor that has 1632 bins which can be used during the classification stage. Figures 5 and 6 illustrate the computation of JML before and after translational invariance.

D. Random Forests (RF) Classifier

Random Forests (RFs) are an ensemble learning method for classification and regression. RFs operate by creating multiple decision trees and outputting the class that is the mode of the classes or mean prediction in the case of the regression task [47]. The first algorithm for random decision was created by Tin Kam Ho. After that, an extension of Ho's algorithm was developed by Breiman et al. [48] which involves combining Breiman's "bagging" idea and random selection of features, introduced first by Ho et. al and resulted in the RFs classifier. The training algorithm for random forests applies the general technique of bootstrap aggregating, or bagging, to tree learners. The number of trees is a free parameter. Typically, a few hundred to several thousand trees are used, depending on the size and nature of the training set.

III. Results and Discussion

In this section, we demonstrate the performance of our approach for classifying 12 CNT classes, defined later. We perform classification using 1000 trees RF classifier, which previously proved to be very efficient [41][39]. During training and testing, we used 5 fold cross-validation, where 80% of data was used for training and the remaining 20% was used for

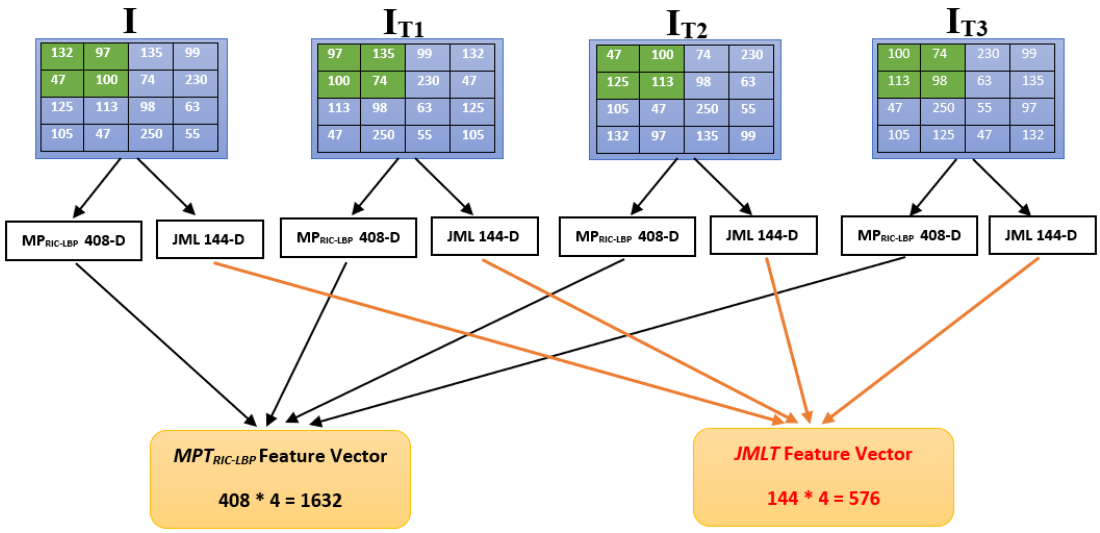

Fig. 6. Computation of JML and MP descriptors after applying three different local translations including one pixel horizontal (T1), one pixel vertical (T2) and one pixel diagonal (t3) for translational invariance.

Fig. 7. Motif Patterns Descriptor Illustration. The Minimum Motif Patterns Matrix is Encoded with RIC-LBP and 408 Bins Features are Extracted.

testing. The evaluation metric used is the Mean Class Accuracy (MCA) which is defined as:

$$MCA = \frac{1}{K}\sum_{K=1}^{K} CCR_k \tag{2}$$

where K is the number of classes and CCR_k is the correct classification rate for each class.

The dimensions of CNT forest images range between 192×730 and 627×730 where rows varies in size as columns have a fixed size. In the experiments, we did not re-size the images or alter them. This is because we are using local feature descriptors that accept any image size. In addition, the number of images per class ranges between 100 - 230.

1) CNT Forest Simulation: CNT forests are simulated for a total number of twelve distinct classes employing three different CNT densities and four outer diameters. Population of CNTs with 250, 500 and 750 CNTs were grown on a 50 μm simulation domain, corresponding to a pitch of 200, 100 and 66.67 nm between CNT nucleation cites, respectively. For simplicity, the outer diameters are 5, 10, 15 and 20 nm, and deemed constant for all CNTs within the forest. CNTs are modeled as hollow cylinders assigned with inner diameters that were 70% of magnitude of outer diameters. The CNT forests were grown up to 1200 total growth steps that corresponds to a height of nearly 55 μm. The CNT growth rate undergoes a sigmoid behavior such that it is highest at the onset of growth,

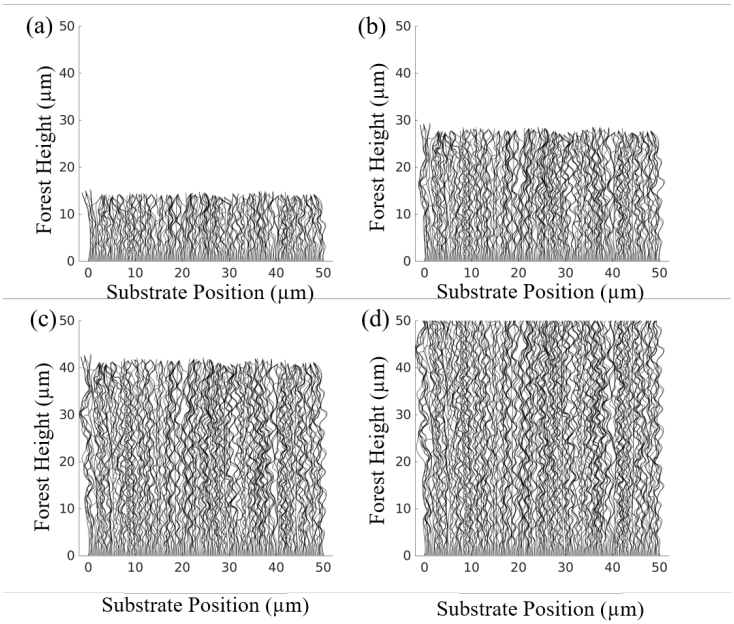

Fig. 8. A typical 500 CNT number forest morphology grown by an average rate of 50 nm/step captured after (a) 300 growth steps (b) 600 growth steps (c) 900 growth steps (d) 1200 growth steps with growth rate of 50 nm per timestep. Simulation time takes around 3 hours for five to ten seconds of CNT growth.

gradually decreases, typically over the subsequent 20 minutes, and finally terminates [49].

However, our ML model training can be trained by simulating CNT forests for a relatively short length, i.e. up to 55 m in this study. This corresponds to the early stages of growth that is fulfilled within a few minutes [49]. Due to computational resources limitations, it takes about a few hours to simulate CNT forests by our finite-element simulation

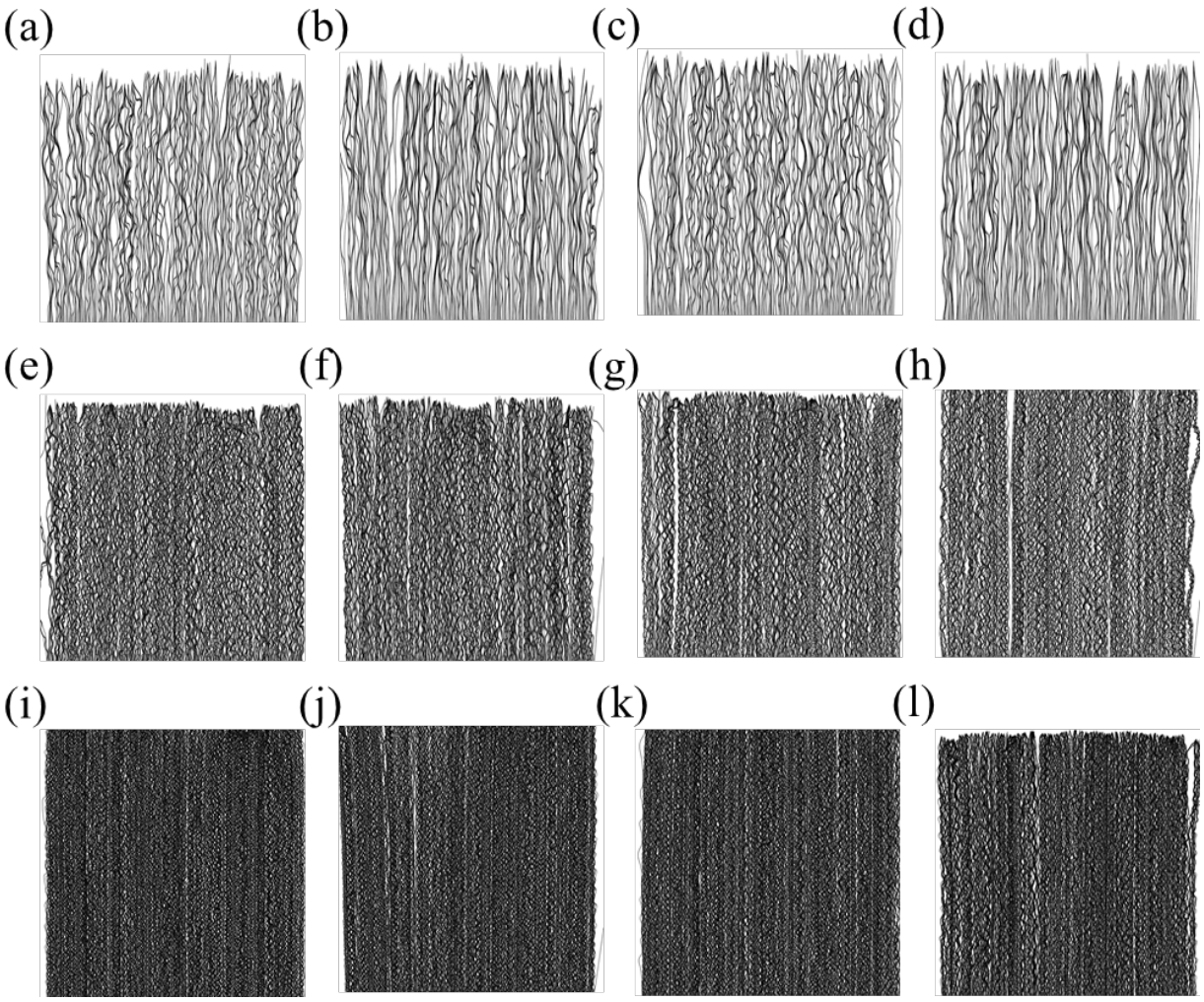

Fig. 9. The CNT forest morphologies (a)class1: 250 CNTs - OD=5 nm (b) class2: 250 CNTs - OD=10 nm (c) class3: 250 CNTs - OD=15 nm (e) class4: 250 CNTs - OD=20 nm (e) class5: 500 CNTs - OD=5 nm (f) class6: 500 CNTs - OD=10 nm (g) class7: 500 CNTs - OD=15 nm (h) class8: 500 CNTs - OD=20 nm (i) class9: 750 CNTs - OD=5 nm (j) class10: 750 CNTs - OD=10 nm (k) class11: 750 CNTs - OD=15 nm (l) class12: 750 CNTs - OD=20 nm.

model. For instance, it takes about 2.5 hours to grow a forest of 55 m height with a pitch of 100 nm between nucleation cites while such forest is grown in less than 2 minutes experimentally [49]. Therefore, the growth rate of each CNT within the population was assigned stochastically from a Gaussian probability density function with an average growth rate of 50 nm per time step and a standard deviation of 5%. The orientation angle of CNTs was also assigned to each CNT based on a Gaussian distribution having a standard deviation of 5° relative to the growth substrate normal. Each class of CNT forests is simulated for several times to generate sufficient amount of data to train the ML model. CNT morphologies are plotted and saved every 100 time steps starting from time step of 300 up to 1200. The first 300 time steps are disregarded due to the short length of forests. A typical forest growth sequence at various time steps is shown in Figure 8. It is interesting that each forest morphology captured during the same forest growth is not exactly similar to the previous morphologies within the same realization.

As discussed earlier, the twelve classes shown above have different densities and outer diameters. A representative image of each CNT forest class may be found in Figure 9. It should be noted that all simulation growth parameters are the same except for the CNT number density and outer diameters. The typical density of a CNT forest is 10^9-10^{13} [18] [19][20][50], while classes 1-to-4 corresponding to Figures 9 (a-d) have CNT number densities of 0.25×10^{10} CNTs/cm^2, that exhibits similar morphology to Figure 1 (b). Classes 5-8 correspond to Figures 9 (e-h) and have CNT number densities of 1×10^{10} CNTs/cm^2. Classes 9-12, as shown in Figures 9 (i-l), have CNT number densities of 2.25×10^{10} CNTs/cm^2, which resembles Figure 1 (a). A summary of synthesis parameters for the twelve class is shown in Table I.

The morphological changes arise from the interactions between adjacent CNTs that make neighboring CNTs bonded by the van der Waals forces and make bundles. The bonds

TABLE I
A SUMMARY OF CNT FOREST SIMULATION GROWTH PARAMETERS WITH AVERAGE GROWTH RATE OF 50 nm PER TIMESTEP AND GROWTH STD OF 5%.

Class No.	Outer Diameter (nm)	Inner Diameter (nm)	CNT Number (/50μm)
1	5	3.5	250
2	10	7.0	250
3	15	10.5	250
4	20	14.0	250
5	5	3.5	500
6	10	7.0	500
7	15	10.5	500
8	20	14.0	500
9	5	3.5	750
10	10	7.0	750
11	15	10.5	750
12	20	14.0	750

are subject to breaking when the generated forces during the forest self-assembly exceed a threshold force of 10 nN [35],[36]. It is worth noting that the x-y axis is cropped in Figure 9 in order to convert plots shown in Figure 8 to images that can be used to train the ML model.

2) Local Features Experiments: Our experiment starts by classifying the CNT forest classes using our framework of four local descriptors: RIC-LBP, JAMBP, JML, and MP. The classification results were reported for each single descriptor as shown in Table II. Then, the combination of descriptors are examined to further improve the classification performance.

TABLE II
RESULTS OF APPLYING OUR LOCAL FEATURES FRAMEWORK USING 1000 TREES RF WITH FIVE-FOLD CROSS VALIDATION. AFTER COMBINING THE FOUR SETS OF FEATURE DESCRIPTORS THE MCA RESULTS IMPROVED BY MORE THAN 3%.

Descriptor	Size	MCA
RIC-LBP	408	80.0
JAMBP	320	76.2
JML	576	80.5
MP	1624	79.4
RIC-LBP + JAMBP	728	79.9
RIC-LBP + JAMBP + JML	1304	81.6
RIC-LBP + JAMBP + JML + MP	2936	83.5

From Table II, the best accuracy of a single local descriptor was obtained by JML. This is because JML uses the spatial relationship among the intensity pixel in a 2×2 neighborhood efficiently. JAMBP exhibited the lowest performance since it was not able to capture the important texture features from the dense tubes of CNT forest. This is mainly because JAMBP proved to work very well with noisy images while CNT forest images are very clean. It is observed that the combination of multiple local descriptors also enhanced the classification performance. In the best case, combining the four descriptors resulted in a performance improvement by more than 3%.

RF classifier with 1000 trees was tested before to classify Human Epithelial type 2 (HEp-2) images and it was very successful in recognizing six and seven classes of cells and specimen samples respectively [39][41]. Hence, the RF classifier was selected to classify CNT forest images that yields impressive results as shown in Table II, when adopting the RF with many trees to aide the voting process within the classifier.

IV. CONCLUSIONS

In this paper, we presented a framework of multiple local descriptors to classify 12 CNT forest classes corresponding to different synthesis conditions. We split the dataset into 5 folds in order to perform 5 fold cross-validation. Then, the Random Forests classifier with 1000 trees was applied on the extracted local descriptors. We have studied several descriptors and demonstrated that the accuracy of a single local descriptor can be improved by concatenating multiple local descriptors and feeding them to the classifier. The accuracy of JML (the best single performance descriptor) was improved from 80.5% to 83.5% by combining all four descriptors: RIC-LBP, JAMBP, JML, and MP. This high classification accuracy promotes discovering the CNT forest synthesis-structure relationships so that their promising performance can be adopted in real world applications. We foresee this work as a meaningful step towards creating an unsupervised simulation using machine learning techniques that can seek out the desired CNT forest synthesis parameters to achieve desired property sets for diverse applications.

ACKNOWLEDGEMENT

The authors would like to acknowledge funding from National Science Foundation (NSF) under award CMMI 1651538 (for TH and MMR).

REFERENCES

[1] G. Dresselhaus, S. Riichiro, *et al.*, *Physical properties of carbon nanotubes*. World scientific, 1998.
[2] X. He, N. Fujimura, J. M. Lloyd, K. J. Erickson, A. A. Talin, Q. Zhang, W. Gao, Q. Jiang, Y. Kawano, R. H. Hauge, *et al.*, "Carbon nanotube terahertz detector," *Nano letters*, vol. 14, no. 7, pp. 3953–3958, 2014.
[3] E. Artukovic, M. Kaempgen, D. Hecht, S. Roth, and G. Grüner, "Transparent and flexible carbon nanotube transistors," *Nano letters*, vol. 5, no. 4, pp. 757–760, 2005.
[4] Q. Cao, H.-s. Kim, N. Pimparkar, J. P. Kulkarni, C. Wang, M. Shim, K. Roy, M. A. Alam, and J. A. Rogers, "Medium-scale carbon nanotube thin-film integrated circuits on flexible plastic substrates," *Nature*, vol. 454, no. 7203, p. 495, 2008.
[5] Z. Wu, Z. Chen, X. Du, J. M. Logan, J. Sippel, M. Nikolou, K. Kamaras, J. R. Reynolds, D. B. Tanner, A. F. Hebard, *et al.*, "Transparent, conductive carbon nanotube films," *Science*, vol. 305, no. 5688, pp. 1273–1276, 2004.
[6] A. M. Jasim, S. E. Hoff, and Y. Xing, "Enhancing methanol electrooxidation activity using double oxide catalyst support of tin oxide clusters on doped titanium dioxides," *Electrochimica Acta*, vol. 261, pp. 221–226, 2018.
[7] Y. Huang, P. V. Palkar, L.-J. Li, H. Zhang, and P. Chen, "Integrating carbon nanotubes and lipid bilayer for biosensing," *Biosensors and Bioelectronics*, vol. 25, no. 7, pp. 1834–1837, 2010.
[8] M. R. Maschmann, B. Dickinson, G. J. Ehlert, and J. W. Baur, "Force sensitive carbon nanotube arrays for biologically inspired airflow sensing," *Smart Materials and Structures*, vol. 21, no. 9, p. 094024, 2012.
[9] M. R. Maschmann, G. J. Ehlert, B. T. Dickinson, D. M. Phillips, C. W. Ray, G. W. Reich, and J. W. Baur, "Bioinspired carbon nanotube fuzzy fiber hair sensor for air-flow detection," *Advanced Materials*, vol. 26, no. 20, pp. 3230–3234, 2014.

[10] T. Yamada, Y. Hayamizu, Y. Yamamoto, Y. Yomogida, A. Izadi-Najafabadi, D. N. Futaba, and K. Hata, "A stretchable carbon nanotube strain sensor for human-motion detection," *Nature nanotechnology*, vol. 6, no. 5, p. 296, 2011.

[11] Y. Gao, T. Kodama, Y. Won, S. Dogbe, L. Pan, and K. E. Goodson, "Impact of nanotube density and alignment on the elastic modulus near the top and base surfaces of aligned multi-walled carbon nanotube films," *Carbon*, vol. 50, no. 10, pp. 3789–3798, 2012.

[12] A. Cao, P. L. Dickrell, W. G. Sawyer, M. N. Ghasemi-Nejhad, and P. M. Ajayan, "Super-compressible foamlike carbon nanotube films," *Science*, vol. 310, no. 5752, pp. 1307–1310, 2005.

[13] M. R. Maschmann, G. J. Ehlert, S. J. Park, D. Mollenhauer, B. Maruyama, A. J. Hart, and J. W. Baur, "Visualizing strain evolution and coordinated buckling within cnt arrays by in situ digital image correlation," *Advanced Functional Materials*, vol. 22, no. 22, pp. 4686–4695, 2012.

[14] M. F. De Volder, S. H. Tawfick, R. H. Baughman, and A. J. Hart, "Carbon nanotubes: present and future commercial applications," *science*, vol. 339, no. 6119, pp. 535–539, 2013.

[15] M. R. Maschmann, Q. Zhang, F. Du, L. Dai, and J. Baur, "Length dependent foam-like mechanical response of axially indented vertically oriented carbon nanotube arrays," *Carbon*, vol. 49, no. 2, pp. 386–397, 2011.

[16] S. B. Hutchens, L. J. Hall, and J. R. Greer, "In situ mechanical testing reveals periodic buckle nucleation and propagation in carbon nanotube bundles," *Advanced Functional Materials*, vol. 20, no. 14, pp. 2338–2346, 2010.

[17] P. Pour Shahid Saeed Abadi, S. B. Hutchens, J. R. Greer, B. A. Cola, and S. Graham, "Buckling-driven delamination of carbon nanotube forests," *Applied Physics Letters*, vol. 102, no. 22, p. 223103, 2013.

[18] M. Bedewy and A. J. Hart, "Mechanical coupling limits the density and quality of self-organized carbon nanotube growth," *Nanoscale*, vol. 5, no. 7, pp. 2928–2937, 2013.

[19] M. Bedewy, E. R. Meshot, M. J. Reinker, and A. J. Hart, "Population growth dynamics of carbon nanotubes," *ACS nano*, vol. 5, no. 11, pp. 8974–8989, 2011.

[20] M. Bedewy, E. R. Meshot, H. Guo, E. A. Verploegen, W. Lu, and A. J. Hart, "Collective mechanism for the evolution and self-termination of vertically aligned carbon nanotube growth," *The Journal of Physical Chemistry C*, vol. 113, no. 48, pp. 20576–20582, 2009.

[21] E. R. Meshot and A. J. Hart, "Abrupt self-termination of vertically aligned carbon nanotube growth," *Applied Physics Letters*, vol. 92, no. 11, p. 113107, 2008.

[22] E. R. Meshot, M. Bedewy, K. M. Lyons, A. R. Woll, K. A. Juggernauth, S. Tawfick, and A. J. Hart, "Measuring the lengthening kinetics of aligned nanostructures by spatiotemporal correlation of height and orientation," *Nanoscale*, vol. 2, no. 6, pp. 896–900, 2010.

[23] J. An, Z. Zhan, and L. Zheng, "Chapter 1 - controllable synthesis of carbon nanotubes," in *Industrial Applications of Carbon Nanotubes* (H. Peng, Q. Li, and T. Chen, eds.), Micro and Nano Technologies, pp. 1 – 45, Boston: Elsevier, 2017.

[24] S. J. Kang, C. Kocabas, T. Ozel, M. Shim, N. Pimparkar, M. A. Alam, S. V. Rotkin, and J. A. Rogers, "High-performance electronics using dense, perfectly aligned arrays of single-walled carbon nanotubes," *Nature nanotechnology*, vol. 2, no. 4, p. 230, 2007.

[25] C. Kocabas, S. J. Kang, T. Ozel, M. Shim, and J. A. Rogers, "Improved synthesis of aligned arrays of single-walled carbon nanotubes and their implementation in thin film type transistors," *The Journal of Physical Chemistry C*, vol. 111, no. 48, pp. 17879–17886, 2007.

[26] Z. Chen, J. Appenzeller, Y.-M. Lin, J. Sippel-Oakley, A. G. Rinzler, J. Tang, S. J. Wind, P. M. Solomon, and P. Avouris, "An integrated logic circuit assembled on a single carbon nanotube," *Science*, vol. 311, no. 5768, pp. 1735–1735, 2006.

[27] S. Wang, Z. Zhang, L. Ding, X. Liang, J. Shen, H. Xu, Q. Chen, R. Cui, Y. Li, and L.-M. Peng, "A doping-free carbon nanotube cmos inverter-based bipolar diode and ambipolar transistor," *Advanced Materials*, vol. 20, no. 17, pp. 3258–3262, 2008.

[28] K. G. Reyes and B. Maruyama, "The machine learning revolution in materials?," *MRS Bulletin*, vol. 44, no. 7, pp. 530–537, 2019.

[29] R. Gómez-Bombarelli, J. Aguilera-Iparraguirre, T. D. Hirzel, D. Duvenaud, D. Maclaurin, M. A. Blood-Forsythe, H. S. Chae, M. Einzinger, D.-G. Ha, T. Wu, *et al.*, "Design of efficient molecular organic light-emitting diodes by a high-throughput virtual screening and experimental approach," *Nature materials*, vol. 15, no. 10, p. 1120, 2016.

[30] J. J. Low, A. I. Benin, P. Jakubczak, J. F. Abrahamian, S. A. Faheem, and R. R. Willis, "Virtual high throughput screening confirmed experimentally: porous coordination polymer hydration," *Journal of the American Chemical Society*, vol. 131, no. 43, pp. 15834–15842, 2009.

[31] O. Obrezanova, G. Csányi, J. M. Gola, and M. D. Segall, "Gaussian processes: a method for automatic qsar modeling of adme properties," *Journal of chemical information and modeling*, vol. 47, no. 5, pp. 1847–1857, 2007.

[32] S. M. Azimi, D. Britz, M. Engstler, M. Fritz, and F. Mücklich, "Advanced steel microstructural classification by deep learning methods," *Scientific reports*, vol. 8, no. 1, p. 2128, 2018.

[33] H. Majidifard, B. Jahangiri, W. G. Buttlar, and A. H. Alavi, "New machine learning-based prediction models for fracture energy of asphalt mixtures," *Measurement*, vol. 135, pp. 438–451, 2019.

[34] Y. Dong, C. Wu, C. Zhang, Y. Liu, J. Cheng, and J. Lin, "Bandgap prediction by deep learning in configurationally hybridized graphene and boron nitride," *npj Computational Materials*, vol. 5, no. 1, p. 26, 2019.

[35] T. Hajilounezhad, D. M. Ajiboye, and M. R. Maschmann, "Evaluating the forces generated during carbon nanotube forest growth and self-assembly," *Materialia*, p. 100371, 2019.

[36] T. Hajilounezhad and M. R. Maschmann, "Numerical investigation of internal forces during carbon nanotube forest self-assembly," in *ASME 2018 International Mechanical Engineering Congress and Exposition*, American Society of Mechanical Engineers, 2018.

[37] M. R. Maschmann, "Integrated simulation of active carbon nanotube forest growth and mechanical compression," *Carbon*, vol. 86, pp. 26–37, 2015.

[38] J. Brown, T. Hajilounezhad, N. T. Dee, S. Kim, A. J. Hart, and M. R. Maschmann, "Delamination mechanics of carbon nanotube micropillars," *ACS applied materials & interfaces*.

[39] V. S. Prasath, Y. M. Kassim, Z. A. Oraibi, J.-B. Guiriec, A. Hafiane, G. Seetharaman, and K. Palaniappan, "HEp-2 cell classification and segmentation using motif texture patterns and spatial features with random forests," in *IEEE Int. Conf. Pattern Recognition*, pp. 90–95, 2016.

[40] Z. A. Oraibi, M. Irio, A. Hafiane, and K. Palaniappan, "Texture classification using multiple local descriptors," in *2017 IEEE Applied Imagery Pattern Recognition Workshop (AIPR)*, pp. 1–7, 2017.

[41] Z. A. Oraibi, H. Yousif, A. Hafiane, G. Seetharaman, and K. Palaniappan, "Learning local and deep features for efficient cell image classification using random forests," in *2018 25th IEEE International Conference on Image Processing (ICIP)*, pp. 2446–2450, 2018.

[42] T. Ojala, M. Pietikainen, and T. Maenpaa, "Multiresolution gray-scale and rotation invariant texture classification with local binary patterns," *IEEE Trans. on Pattern Analysis and Machine Intelligence*, vol. 24, no. 7, pp. 971–987, 2002.

[43] A. Hafiane, S. Chaudhuri, G. Seetharaman, and B. Zavidovique, "Region-based CBIR in GIS with local space filling curves to spatial representation," *Pattern Recognition Letters*, vol. 27, no. 4, pp. 259–267, 2006.

[44] R. Nosaka and K. Fukui, "HEp-2 cell classification using rotation invariant co-occurrence among local binary patterns," *Pattern Recognition*, vol. 47, no. 7, pp. 2428–2436, 2014.

[45] A. Hafiane, K. Palaniappan, and G. Seetharaman, "Joint adaptive median binary patterns for texture classification," *Pattern Recognition*, vol. 48, no. 8, pp. 2609–2620, 2015.

[46] A. Hafiane, K. Palaniappan, and G. Seetharaman, "Adaptive median binary patterns for texture classification," in *International Conference on Pattern Recognition*, pp. 1138–1143, 2014.

[47] T. K. Ho, "Random decision forests," in *International conference on Document Analysis and Recognition*, vol. 1, pp. 278–282, 1995.

[48] L. Breiman, "Bagging predictors," *Machine Learning*, vol. 24, pp. 123–140, Aug 1996.

[49] D. N. Futaba, K. Hata, T. Yamada, K. Mizuno, M. Yumura, and S. Iijima, "Kinetics of water-assisted single-walled carbon nanotube synthesis revealed by a time-evolution analysis," *Physical Review Letters*, vol. 95, no. 5, p. 056104, 2005.

[50] G. Zhong, J. H. Warner, M. Fouquet, A. W. Robertson, B. Chen, and J. Robertson, "Growth of ultrahigh density single-walled carbon nanotube forests by improved catalyst design," *ACS nano*, vol. 6, no. 4, pp. 2893–2903, 2012.